

Backward single-pion production in the $pd \rightarrow {}^3\text{He} \pi^0$ reaction with WASA-at-COSY

The WASA-at-COSY Collaboration

P. Adlarson¹, W. Augustyniak², W. Bardan³, M. Bashkanov⁴, F.S. Bergmann⁵, M. Berłowski⁶, A. Bondar^{7,8}, M. Büscher^{9,10}, H. Calén¹, I. Ciepał¹¹, H. Clement^{12,13}, E. Czerwiński³, K. Demmich⁵, R. Engels¹⁴, A. Erven¹⁵, W. Erven¹⁵, W. Eyrych¹⁶, P. Fedorets^{14,17}, K. Föhl¹⁸, K. Fransson¹, F. Goldenbaum¹⁴, A. Goswami^{14,19}, K. Grigoryev^{14,20}, C.-O. Gullström¹, L. Heijkenkjöld^{1,a}, V. Hejny¹⁴, N. Hüskens^{5,b}, L. Jarczyk³, T. Johansson¹, B. Kamys³, G. Kemmerling^{15,c}, G. Khatiri^{3,d}, A. Khoukaz⁵, A. Khreptak³, D.A. Kirillov²¹, S. Kistryn³, H. Kleines^{15,e}, B. Klos²², W. Krzemień⁶, P. Kulessa¹¹, A. Kupś^{1,6}, A. Kuzmin^{7,8}, K. Lalwani²³, D. Lersch¹⁴, B. Lorentz¹⁴, A. Magiera³, R. Maier^{14,24}, P. Marciniowski¹, B. Mariański², H.-P. Morsch², P. Moskal³, H. Ohm¹⁴, W. Parol¹¹, E. Perez del Rio^{12,13,f}, N.M. Piskunov²¹, D. Prasuhn¹⁴, D. Pszczel^{1,6}, K. Pysz¹¹, A. Pyszniak^{1,3}, J. Ritman^{14,24,25}, A. Roy¹⁹, Z. Rudy³, O. Rundel³, S. Sawant²⁵, S. Schadmand¹⁴, I. Schätti-Ozerianska³, T. Sefzick¹⁴, V. Serdyuk¹⁴, B. Shwartz^{7,8}, K. Sitterberg⁵, T. Skorodko^{12,13,26}, M. Skurzok³, J. Smyrski³, V. Sopov¹⁷, R. Stassen¹⁴, J. Stepaniak⁶, E. Stephan²², G. Sterzenbach¹⁴, H. Stockhorst¹⁴, H. Ströher^{14,24}, A. Szczurek¹¹, A. Trzciński², M. Wolke¹, A. Wrońska³, P. Wüstner¹⁵, A. Yamamoto²⁷, J. Zabierowski²⁸, M.J. Zieliński³, J. Złomańczuk¹, P. Żuprański², M. Żurek¹⁴, and C. Wilkin²⁹

- ¹ Division of Nuclear Physics, Department of Physics and Astronomy, Uppsala University, Box 516, 75120 Uppsala, Sweden
- ² Department of Nuclear Physics, National Centre for Nuclear Research, ul. Hoza 69, 00-681, Warsaw, Poland
- ³ Institute of Physics, Jagiellonian University, prof. Stanisława Łojasiewicza 11, 30-348 Kraków, Poland
- ⁴ School of Physics and Astronomy, University of Edinburgh, James Clerk Maxwell Building, Peter Guthrie Tait Road, Edinburgh EH9 3FD, UK
- ⁵ Institut für Kernphysik, Westfälische Wilhelms-Universität Münster, Wilhelm-Klemm-Str. 9, 48149 Münster, Germany
- ⁶ High Energy Physics Department, National Centre for Nuclear Research, ul. Hoza 69, 00-681, Warsaw, Poland
- ⁷ Budker Institute of Nuclear Physics of SB RAS, 11 akademika Lavrentieva prospect, Novosibirsk, 630090, Russia
- ⁸ Novosibirsk State University, 2 Pirogova Str., Novosibirsk, 630090, Russia
- ⁹ Peter Grünberg Institut, PGI-6 Elektronische Eigenschaften, Forschungszentrum Jülich, 52425 Jülich, Germany
- ¹⁰ Institut für Laser- und Plasmaphysik, Heinrich-Heine Universität Düsseldorf, Universitätsstr. 1, 40225 Düsseldorf, Germany
- ¹¹ The Henryk Niewodniczański Institute of Nuclear Physics, Polish Academy of Sciences, Radzikowskiego 152, 31-342 Kraków, Poland
- ¹² Physikalisches Institut, Eberhard-Karls-Universität Tübingen, Auf der Morgenstelle 14, 72076 Tübingen, Germany
- ¹³ Kepler Center für Astro- und Teilchenphysik, Physikalisches Institut der Universität Tübingen, Auf der Morgenstelle 14, 72076 Tübingen, Germany
- ¹⁴ Institut für Kernphysik, Forschungszentrum Jülich, 52425 Jülich, Germany
- ¹⁵ Zentralinstitut für Engineering, Elektronik und Analytik, Forschungszentrum Jülich, 52425 Jülich, Germany
- ¹⁶ Physikalisches Institut, Friedrich-Alexander-Universität Erlangen-Nürnberg, Erwin-Rommel-Str. 1, 91058 Erlangen, Germany
- ¹⁷ Institute for Theoretical and Experimental Physics named after A.I. Alikhanov of National Research Centre “Kurchatov Institute”, 25 Bolshaya Chermushkinskaya, Moscow, 117218, Russia
- ¹⁸ II. Physikalisches Institut, Justus-Liebig-Universität Gießen, Heinrich-Buff-Ring 16, 35392 Giessen, Germany
- ¹⁹ Department of Physics, Indian Institute of Technology Indore, Khandwa Road, Simrol, Indore - 453552, Madhya Pradesh, India
- ²⁰ High Energy Physics Division, Petersburg Nuclear Physics Institute named after B.P. Konstantinov of National Research Centre “Kurchatov Institute”, 1 mkr. Orlova roshcha, Leningradskaya Oblast, Gatchina, 188300, Russia
- ²¹ Veksler and Baldin Laboratory of High Energy Physics, Joint Institute for Nuclear Physics, 6 Joliot-Curie, Dubna, 141980, Russia
- ²² August Chelkowski Institute of Physics, University of Silesia, Uniwersytecka 4, 40-007, Katowice, Poland
- ²³ Department of Physics, Malaviya National Institute of Technology Jaipur, JLN Marg Jaipur - 302017, Rajasthan, India
- ²⁴ JARA-FAME, Jülich Aachen Research Alliance, Forschungszentrum Jülich and RWTH Aachen - Jülich, Aachen, Germany
- ²⁵ Institut für Experimentalphysik I, Ruhr-Universität Bochum, Universitätsstr. 150, 44780 Bochum, Germany
- ²⁶ Department of Physics, Tomsk State University, 36 Lenina Avenue, Tomsk, 634050, Russia

²⁷ High Energy Accelerator Research Organisation KEK, Tsukuba, Ibaraki 305-0801, Japan

²⁸ Astrophysics Division, National Centre for Nuclear Research, Box 447, 90-950 Łódź, Poland

²⁹ Physics and Astronomy Department, UCL, Gower Street, London WC1E 6BT, UK

Received: 21 May 2018 / Revised: 7 August 2018

Published online: 17 September 2018

© Società Italiana di Fisica / Springer-Verlag GmbH Germany, part of Springer Nature, 2018

Communicated by U.-G. Meißner

Abstract. New data on the production of single neutral pions in the $pd \rightarrow {}^3\text{He} \pi^0$ reaction are presented. For fifteen proton beam momenta between $p_p = 1.60 \text{ GeV}/c$ and $p_p = 1.74 \text{ GeV}/c$, differential cross sections are determined over a large fraction of the backward hemisphere. Since the only previous systematic measurements of single-pion production at these energies were made in collinear kinematics, the present work constitutes a significant extension of the current knowledge on this reaction. Even this far above the production threshold, significant changes are found in the behaviour of the angular distributions over small intervals in beam momentum.

1 Introduction

In contrast to other meson production reactions in proton-deuteron fusion, most notably the η - and $(\pi\pi)^0$ -channels, the production of single, neutral pions in the reaction $pd \rightarrow {}^3\text{He} \pi^0$ is considerably less well studied in the energy region around the η -production threshold. Early measurements of the cross section (see fig. 1) and tensor analysing power of the $pd(dp) \rightarrow {}^3\text{He} \pi^0$ and $pd \rightarrow {}^3\text{H} \pi^+$ reactions in collinear kinematics with the SPES4 spectrometer at SATURNE [1,2] revealed strong structures in both observables for backward pion production (with respect to the direction of the incident proton in the c.m. frame) around $p_p = 1.70 \text{ GeV}/c$. It is important to note here that, since there is only one isospin amplitude, the cross section for $pd \rightarrow {}^3\text{H} \pi^+$ should be twice that for $pd \rightarrow {}^3\text{He} \pi^0$, though deviations of the order of 10% have been reported in the literature [3,4].

Apart from a single measurement of $dp \rightarrow {}^3\text{He} \pi^0$ at $p_d = 3.5 \text{ GeV}/c$ [5], angular distributions in the η -threshold region (corresponding to a proton beam momentum of $p_p = 1.572 \text{ GeV}/c$ and an excess energy of $Q_{\pi^0} = 412.9 \text{ MeV}$ above the single pion threshold) have so far remained largely unexplored. Nevertheless, the extensive database of cross sections for collinear production, combined with the similarities of the ${}^3\text{He}$ detection in the reactions $pd \rightarrow {}^3\text{He} \eta$ and $pd \rightarrow {}^3\text{He} \pi^0 \pi^0$, have made $pd \rightarrow {}^3\text{He} \pi^0$ a prime candidate for luminosity determinations in fusion reactions [6,7]. There is, thus, a twofold motivation for extended studies of differential cross sections of the $pd \rightarrow {}^3\text{He} \pi^0$ reaction. These will permit an exploration of the variations close to $\cos \vartheta_{\pi^0}^* = -1$ in the vicinity of the η -production threshold as well as the estab-

lishment of a new database for future experiments, that does not rely on an extrapolation to collinear kinematics. Data obtained in parallel to the WASA-at-COSY experiment on η -production away from threshold [8] allow a detailed study of the cross sections for single-pion production over a significant part of the backward hemisphere.

There have been several attempts to describe the $pd \rightarrow {}^3\text{He} \pi^0$ data but these have mainly concentrated on the low energy region where many experiments had been carried out. The simplest of these is the quasi-deuteron model, first discussed by Ruderman [9]. Here it is assumed that the reaction takes place through quasi-free $pn \rightarrow d\pi^0$ on a neutron in the deuterium target followed by the capture of the deuteron on the spectator proton to form the observed ${}^3\text{He}$. Detailed numerical studies have been carried out by Falk [10] and Canton and Levchuk [11] but it has been pointed out [12] that there are also important contributions from spin-singlet NN waves as well as the spin-triplet deuteron. Though calculations at higher energies are hampered by the limited knowledge of the $pn \rightarrow d\pi^0$ amplitude structure at beam energies above 800 MeV, it is likely that spectator models will be less important. Genuine three-nucleon processes have been invoked to explain η production in the $pd \rightarrow {}^3\text{He} \eta$ reaction [13] and it seems likely that analogous effects will be important in the description of our new and detailed data.

2 Experiment

The π^0 data were obtained at the WASA facility located within the Cooler Synchrotron (COSY) of the Forschungszentrum Jülich in the same experiment as that designed

^a Present Address: Institut für Kernphysik, Johannes Gutenberg-Universität Mainz, Johann-Joachim-Becher Weg 45, 55128 Mainz, Germany.

^b e-mail: n.hues02@uni-muenster.de (corresponding author)

^c Present Address: Jülich Centre for Neutron Science JCNS, Forschungszentrum Jülich, 52425 Jülich, Germany.

^d Present Address: Department of Physics, Harvard University, 17 Oxford St., Cambridge, MA 02138, USA.

^e Present Address: Jülich Centre for Neutron Science JCNS, Forschungszentrum Jülich, 52425 Jülich, Germany.

^f Present Address: INFN, Laboratori Nazionali di Frascati, Via E. Fermi, 40, 00044 Frascati (Roma), Italy

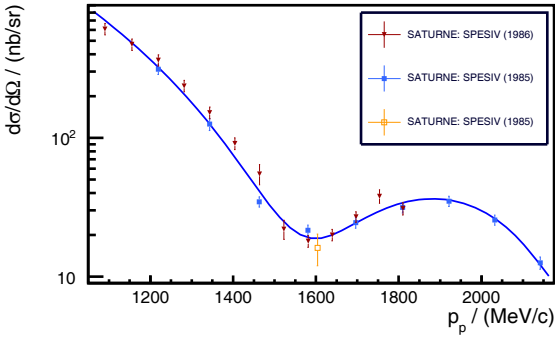


Fig. 1. Differential cross sections of the reactions $pd \rightarrow {}^3\text{He}\pi^0$ and $pd \rightarrow {}^3\text{H}\pi^+$ (scaled by an isospin factor of 0.5) at $\cos\vartheta_{\pi^0}^* = -1$ [1, 2]. The curve represents a fourth order polynomial fit to the combined database.

to study η production [8]. Beam protons were steered to collide with pellets of frozen deuterium and the heavy ${}^3\text{He}$ ejectiles of interest were emitted near the forward direction in the laboratory frame. The WASA Forward Detector allows the energy and the polar (θ) and azimuthal (ϕ) angles of the ${}^3\text{He}$ nuclei to be reconstructed in multiple layers of plastic scintillators and a proportional chamber, respectively. Angular coverage ranges from approximately 3° to 17° in ϑ and a full 360° in φ with an angular resolution of $\Delta\vartheta = 0.2^\circ$ [14]. The energy resolution is approximately 3% for particles stopped within the detector and between 4% and 8% for particles punching through the full forward detector [14]. The main device for the energy measurement during this measurement is the Forward Range Hodoscope, consisting of three layers of plastic scintillator with a thickness of 11 cm each. Additional and more detailed information on the experimental setup can be found in ref. [14].

Fifteen evenly spaced proton beam momenta were used between $p_p = 1.60 \text{ GeV}/c$ and $p_p = 1.74 \text{ GeV}/c$, with a resolution of $\Delta p/p \approx 10^{-3}$ [15]. Utilising the so-called supercycle mode of the accelerator, data can be taken at eight different beam momentum settings, with multiple repeats one after another, thus minimising systematic differences between the individual measurements. Two such supercycles were employed in this experiment. The measurement at $p_p = 1.70 \text{ GeV}/c$ was repeated in both supercycles and an additional single-momentum measurement was made at this momentum to allow systematic effects between the two supercycles to be investigated. During the analysis, the three measurements at $1.70 \text{ GeV}/c$ were treated fully independently and no deviations were found between their results. This implies that there are no systematic uncertainties due to environmental changes between the measurement periods and the three sets of data at $1.70 \text{ GeV}/c$ could be combined.

3 Analysis

The ${}^3\text{He}$ nuclei produced near the forward direction are identified in the WASA Forward Detector by means of

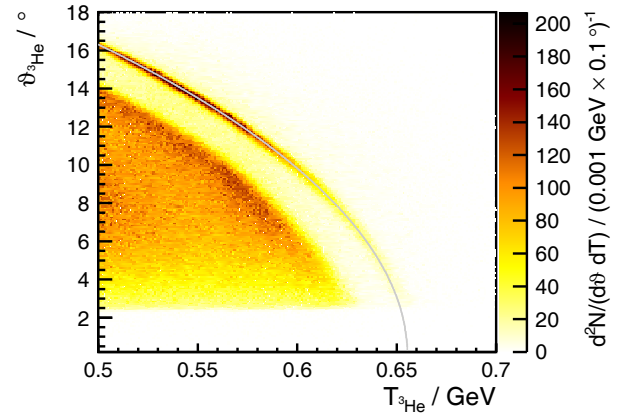


Fig. 2. Production angle of ${}^3\text{He}$ nuclei in the laboratory frame displayed as a function of their kinetic energy. The two-dimensional plot represents data (with colour indicating the event yield), whereas the grey line follows from applying four-momentum conservation to the $pd \rightarrow {}^3\text{He}\pi^0$ reaction. The single pion production is kinematically separated from two- (and three-) pion production, whose kinematic edge is clearly visible.

their energy loss. In the case of single-pion production, only those ${}^3\text{He}$ nuclei that stopped in the second layer of the Forward Range Hodoscope are considered. From this energy loss, a first value of the kinetic energy $T_{{}^3\text{He}}$ can be estimated by comparison with a Monte Carlo simulation of the π^0 production reaction. By measuring also the polar and azimuthal production angles ϑ and φ in the Forward Proportional Chamber, the four-momenta of the ${}^3\text{He}$ nuclei are fully determined so that a missing-mass analysis could be performed. The analytic relation between the precisely measured polar scattering angle ($\Delta\vartheta \approx 0.2^\circ$) and the kinetic energy of ${}^3\text{He}$ nuclei was exploited in order to carefully monitor the energy calibration (see fig. 2).

Even though the detector system was capable of measuring photons from the decay of the π^0 , for the studies reported here, only the ${}^3\text{He}$ in the final state was used, with the π^0 being identified effectively through a missing-mass analysis. The angular distribution of the single-pion production is derived from the spectra of final state momentum, which are treated bin-wise in $\cos\vartheta_{\pi^0}^*$. A typical example of such a spectrum, with an angular bin-width of $\Delta\cos\vartheta_{\pi^0}^* = 0.016$, can be found in fig. 3. The background, largely associated with two-pion production and single-pion production with a poorly reconstructed energy due to the breakup of ${}^3\text{He}$ nuclei in the scintillator material, is subtracted using a fit of the type

$$f(x) = e^{a(x-0.5)}(b + cx + dx^2), \quad (1)$$

where x is the ${}^3\text{He}$ c.m. momentum in GeV/c . The fit is made outside the π^0 peak region.

There is no strong variation of the background with $\cos\vartheta_{\pi^0}^*$, apart from the largest values of $\cos\vartheta_{\pi^0}^*$ at each beam momentum, for which two-pion production no longer fulfills the requirement of a ${}^3\text{He}$ nucleus stopped in the second layer of the Forward Range Hodoscope. The resolution in the c.m. momentum increases slightly for

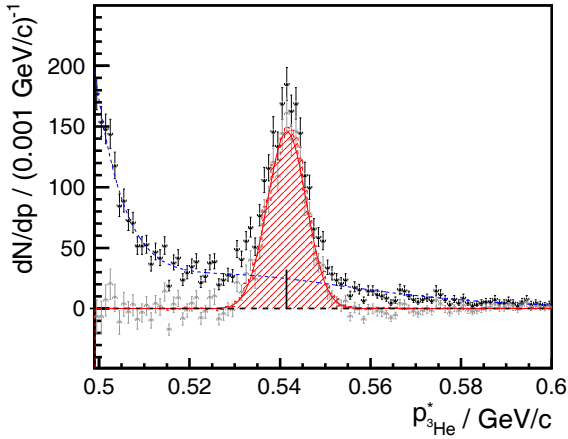


Fig. 3. Spectrum of the final state momentum p_{He}^* of ${}^3\text{He}$ nuclei in the centre-of-mass system for $-0.856 \leq \cos \vartheta_{\pi^0}^* < -0.840$ at a laboratory beam momentum of $p_p = 1.70 \text{ GeV}/c$. Black upward triangles represent data. The blue dashed line is a fit of the type given in eq. (1) to the spectrum, excluding the peak region. Grey downward triangles show the data after subtraction of the background fit. The π^0 peak is fitted by a Gaussian distribution (continuous red line) and compared to a Monte Carlo simulation of the $pd \rightarrow {}^3\text{He}\pi^0$ reaction (red shaded histogram). The nominal peak position for a beam momentum of $p_p = 1.70 \text{ GeV}/c$ is indicated by the vertical solid black line.

larger values of $\cos \vartheta_{\pi^0}^*$, while at the same time the resolution of $\cos \vartheta_{\pi^0}^*$ itself decreases. Both of these measurements depend on the energy and polar angle of the ${}^3\text{He}$ in the laboratory frame. However, for $\cos \vartheta_{\pi^0}^*$ close to -1.0 , the resolution of the c.m. momentum is largely determined by the energy reconstruction, whereas the $\cos \vartheta_{\pi^0}^*$ resolution is largely determined by the angle reconstruction (and vice versa for $\cos \vartheta_{\pi^0}^*$ approaching zero). It should be mentioned here that the resolution in $\cos \vartheta_{\pi^0}^*$ is at worse around 0.008, so that the choice of bin-width of $\Delta \cos \vartheta_{\pi^0}^* = 0.016$ is based entirely on the available statistics.

The effect of nuclear breakup of the ${}^3\text{He}$ within the detector is accounted for in a Monte Carlo simulation using an extension to GEANT3 [16], originally developed for the work in ref. [17] (see also appendix A). A fit of a Gaussian to the background-subtracted data is used to define a $\pm 3\sigma$ environment around the peak position. The event yield within a certain bin in $\cos \vartheta_{\pi^0}^*$ is then defined as the integral of the background-subtracted data in the $\pm 3\sigma$ interval.

As no information is available on the angular distribution of single-pion production, the product of acceptance and reconstruction efficiency (for simplicity called below the *acceptance* $A(\cos \vartheta_{\pi^0}^*)$) is first derived from a Monte Carlo simulation of π^0 production, assuming that the events are uniformly distributed over phase-space. The angular distributions found in the experiment are corrected for the acceptance by bin-wise multiplication with $A^{-1}(\cos \vartheta_{\pi^0}^*)$. A polynomial fit of fourth order to these distributions is subsequently used to weight the Monte Carlo

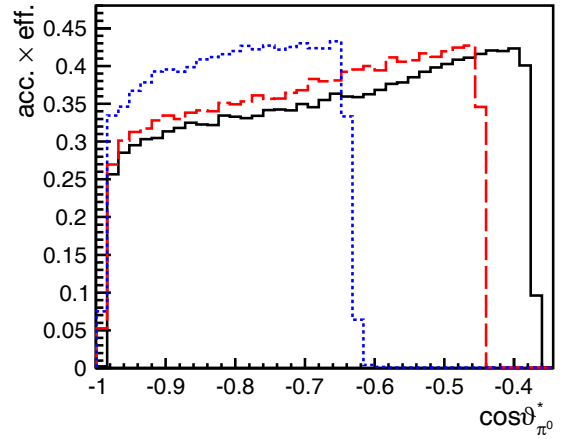


Fig. 4. Product of acceptance and reconstruction efficiency $A(\cos \vartheta_{\pi^0}^*)$ for the $pd \rightarrow {}^3\text{He}\pi^0$ reaction as function of the c.m. production angle for beam momenta of $p_p = 1.60 \text{ GeV}/c$ (blue, short-dashed line), $p_p = 1.70 \text{ GeV}/c$ (red long-dashed line) and $p_p = 1.74 \text{ GeV}/c$ (black, solid line).

simulations. This procedure is repeated until there is convergence of $A(\cos \vartheta_{\pi^0}^*)$, when the angular distributions are determined. This method was applied separately for the measurements at all 15 beam momenta.

Examples of the resulting acceptance as a function of $\cos \vartheta_{\pi^0}^*$ are displayed in fig. 4 for the measurements at $1.60 \text{ GeV}/c$, $1.70 \text{ GeV}/c$ and $1.74 \text{ GeV}/c$. At very large negative values of $\cos \vartheta_{\pi^0}^*$, the beam pipe in the detector limits the acceptance, whereas for the smallest value of $\vartheta_{\pi^0}^*$ the polar production angle ϑ_{He} exceeds the geometrical coverage of the Forward Detector. On average, the angle-dependent acceptance $A(\cos \vartheta_{\pi^0}^*)$ is of the order of 40%. This relatively small value is due mainly to the nuclear breakup of the ${}^3\text{He}$ ions in the scintillator, leading to either a misidentification or a poorly reconstructed kinetic energy.

4 Normalisation

Since the data reported here were taken in parallel to those used to investigate η production in pd fusion, the same normalisation methodology can be applied [8], and this is briefly summarised. A relative normalisation is first derived from the ratio of protons elastically scattered off the target deuteron at a certain beam momentum and the reference momentum $p_p = 1.70 \text{ GeV}/c$. The luminosity for the measurement at $p_p = 1.70 \text{ GeV}/c$ is obtained by normalisation to the measured $pd \rightarrow {}^3\text{He}\eta$ total cross section [18]. The statistical uncertainty of the luminosity determination is of the order of 2% but an additional systematic normalisation uncertainty of $\approx 16\%$ needs to be taken into consideration. This arises from the uncertainty of the reference data [18] and the differences that are apparent when cross sections in different parts of phase-space are used for normalisation instead of the total cross section. For more information on the normalisation procedure, the reader is referred to refs. [8, 19].

5 Results

Angular distributions of single-pion production in proton-deuteron fusion are converted into the differential cross sections shown in fig. 5 using the luminosities previously derived [8, 19]. Apart from the normalisation, the two main sources of the remaining systematic uncertainty, shown by the grey histogram in fig. 5, are minor imprecisions in the determination of the polar production angle (with a possible offset of $\pm 0.04^\circ$) and the distribution of residual gas within the WASA scattering chamber. However, a comparison with the available data for collinear production reveals good agreement, especially if the normalisation uncertainties of both the present data and those from the Saclay experiments [1, 2] are taken into account. To show this more clearly, the combined normalisation uncertainty is incorporated into the error bars of the grey circles in fig. 5. Numerical values of the data are presented in tables 2 and 3, given in appendix B.

The data shown in fig. 5 can be well fit with the fourth order polynomial

$$\frac{d\sigma}{d\Omega} = \sum_{n=0}^{n=4} a_n (\cos \vartheta_{\pi^0}^* + 1)^n \quad (2)$$

and the values of the parameters a_n are to be found in table 1 for the fifteen different beam momenta. Error bars are not shown because they are very misleading in view of the very strong correlations between the parameters and the dependence of the parameters on the degree of the polynomial. In view of this, the energy dependence of the parameters a_3 and a_4 for small proton beam momenta is not statistically significant. Nevertheless, the parametrisation of the data with eq. (2) gives a good description of our results that can be used in the normalisation of other experiments. It should, however, be emphasised that these fits to the observed differential cross section do not provide robust predictions in regions that have not been measured.

For all the data above about 1.66 GeV/c there is clear evidence for a minimum in the differential cross section close to $\cos \vartheta_{\pi^0}^* = -1$. However, the fit parameters of table 1 show that at lower momenta there may also be a minimum but in the unphysical region of $\cos \vartheta_{\pi^0}^* < -1$. The minimum therefore moves somewhat with beam momentum from $\cos \vartheta_{\pi^0}^* \approx -1.1$ at $p_p = 1.62$ GeV/c to -0.93 at 1.74 GeV/c. In contrast, the maximum seen in fig. 5 hardly moves from its position at $\cos \vartheta_{\pi^0}^* \approx -0.61$.

In general, six independent helicity amplitudes are required to describe completely the $pd \rightarrow {}^3\text{He}\pi^0$ reaction. These reduce to two, A and B , in the forward and backward directions and the magnitudes of these, $|A|^2$ and $|B|^2$, can be deduced from the Saclay measurements of the differential cross section and deuteron tensor analysing power T_{20} [2]. At $\vartheta_{\pi^0}^* = 180^\circ$ both $|A|^2$ and $|B|^2$ show minima for proton beam momenta around 1600 to 1650 MeV/c. This behaviour, which causes rapid variations in T_{20} , must clearly be linked to the moving minima shown by our data in fig. 5.

It may also be relevant that the proton analysing power in the $\bar{p}d \rightarrow {}^3\text{He}\pi^0$ reaction at fixed pion angle of $\vartheta_{\pi^0}^* = 170^\circ$ shows an extremely rapid variation with the proton beam momentum in the 1600 MeV/c region [20]. There is therefore much structure in large angle $pd \rightarrow {}^3\text{He}\pi^0$ data near the η threshold and it is tempting to wonder whether this is more than an accident.

The amplitude for the $pd \rightarrow {}^3\text{He}\eta$ reaction near threshold is anomalously strong [21, 22] and might be an indication of the formation of a quasibound ${}^3\text{He}$ state [23]. There might therefore be an extra S -wave contribution caused by η production followed by the transmutation $\eta {}^3\text{He} \rightarrow {}^3\text{He}\pi^0$ that will interfere with a direct mechanism. However, using data on $\pi^- {}^3\text{He} \rightarrow {}^3\text{H}\eta$ [24], it seems that this two-step approach may be too small to explain the backward minima. However, there is no valid reason to retain only the ${}^3\text{He}$ ground state in the intermediate state. Further theoretical work will be needed to explore this interesting region.

6 Summary

Measurements of the differential cross sections of single-pion production in proton-deuteron fusion have been reported here for fifteen different proton beam momenta between 1.60 GeV/c and 1.74 GeV/c. These data, which cover a large part of the backward hemisphere, are a significant extension of the current database that in this momentum region contained only detailed information for collinear production. Despite the data being taken far above the π^0 production threshold, where the excess energy is limited by $426 \text{ MeV} < Q_{\pi^0} < 494 \text{ MeV}$, there are important changes in the angular distributions with increasing Q_{π^0} . In particular at the lowest energy the large angle minimum is at an unphysical point but it becomes observable with rising Q_{π^0} . This and other phenomena [2, 20] seem to occur close to the threshold for η production. Much more theoretical work will be required to see if this is more than a coincidence.

Irrespective of the interpretation of the observed angular distributions, the new data will be a valuable tool for normalising the cross sections for other meson production reactions in proton-deuteron fusion. These data, which are parametrised in eq. (2) and table 1, will avoid having to rely on any extrapolation to collinear kinematics. However, it is dangerous to use the fits in angular regions that have not been measured.

The work presented here received funding from the European Union Seventh Framework Programme (FP7/2007-2013) under grant agreement number 283286. The support given by the Forschungszentrum Jülich FFE Funding Programme of the Jülich Centre for Hadron Physics, by the Polish National Science Centre through grant No. 2016/23/B/ST2/00784, and by the DFG through the Research Training Group GRK2149 is gratefully acknowledged. We thank the COSY crew for their work and the excellent conditions made available during the beam time.

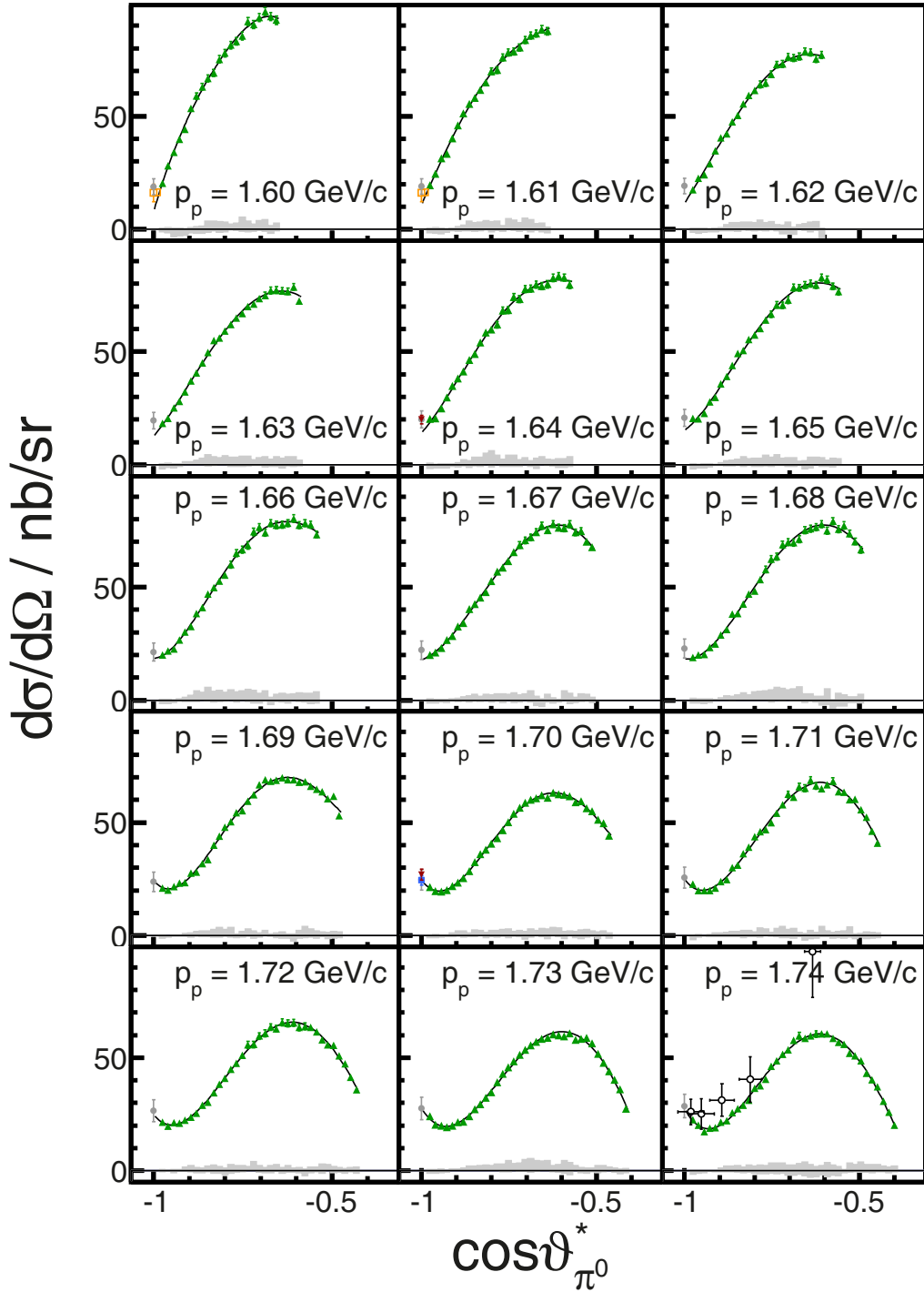


Fig. 5. Differential cross sections of the $pd \rightarrow {}^3\text{He}\pi^0$ reaction in the backward hemisphere for the different values of the beam momentum p_p noted in each panel. Green upward triangles represent the present data, yellow empty boxes a measurement at $p_p = 1.604 \text{ GeV}/c$ [1], the blue filled box a measurement of $pd \rightarrow {}^3\text{H}\pi^+$ at $p_p = 1.697 \text{ GeV}/c$ (scaled by an isospin factor of 0.5) [1], red downward triangles the measurements of $dp \rightarrow {}^3\text{He}\pi^0$ at $p_d = 3.276 \text{ GeV}/c$ and $p_d = 3.392 \text{ GeV}/c$ [2], and the black empty circles the measurement of $dp \rightarrow {}^3\text{He}\pi^0$ at $p_d = 3.50 \text{ GeV}/c$ [5]. In addition, the grey filled circles represent the values of a fit to the combined database shown in fig. 1 at the appropriate beam momentum. In the last case the error bars are composed of the statistical uncertainty of the fit as well as of the normalisation uncertainty of both the present experiment and the literature data. Black solid lines represent fits of the type given in eq. (2). Normalisation uncertainties of the individual datasets are not displayed. The grey histograms represent the systematic uncertainties, other than normalisation, of the present measurements. Numerical values of the data are presented in appendix B.

Table 1. Values of the parameters a_n obtained from fits to our data using eq. (2) for the different beam momenta p_p and excess energies Q_{π^0} in the ${}^3\text{He}\pi^0$ final state.

p_p	Q_{π^0}	a_0	a_1	a_2	a_3	a_4	χ^2/ndf
GeV/c	MeV	nb/sr					
1.60	426.5	7.99	548	-1566	4124	-6096	14.0/16
1.61	431.3	10.83	358	-122	-1447	1910	12.2/17
1.62	436.1	11.63	231	523	-2585	2117	16.4/19
1.63	440.9	12.65	190	645	-2464	1608	16.0/20
1.64	445.7	14.25	171	793	-2918	2294	19.9/21
1.65	450.5	15.25	114	1024	-3053	1968	28.0/22
1.66	455.3	18.47	10	1787	-5147	3886	17.3/23
1.67	460.1	17.92	49	1067	-2433	960	12.5/25
1.68	464.9	18.38	-30	1610	-3776	2155	27.4/26
1.69	469.7	24.43	-188	2612	-6461	4528	32.7/27
1.70	474.5	24.43	-200	2392	-5601	3680	35.8/28
1.71	479.3	25.04	-203	2316	-4978	2807	36.1/29
1.72	484.1	24.67	-188	2199	-4779	2743	16.2/30
1.73	488.9	27.70	-254	2259	-4434	2255	27.5/31
1.74	493.7	27.47	-285	2621	-5545	3230	25.8/32

Appendix A. ${}^3\text{He}$ -detector interactions

Within the GEANT3 framework, the interaction of ${}^3\text{He}$ nuclei (in contrast to p , d and ${}^4\text{He}$ nuclei) with detector material is limited to electromagnetic processes [16]. The authors of [17] extended the description of ${}^3\text{He}$ interactions by incorporating hadronic energy loss and discrete breakup processes. The energy loss of ${}^3\text{He}$ nuclei in the WASA Forward Detector is displayed in fig. 6 for a Monte Carlo simulation of ${}^3\text{He}$ nuclei evenly distributed in kinetic energy between $0.1\text{ GeV} \leq T_{{}^3\text{He}} \leq 0.9\text{ GeV}$ and between $2^\circ \leq \vartheta \leq 20^\circ$ in polar production angle. A comparison of simulations without the proper incorporation of ${}^3\text{He}$ -detector interactions (fig. 6, top) and using the extension provided by the authors of [17] (fig. 6, bottom)

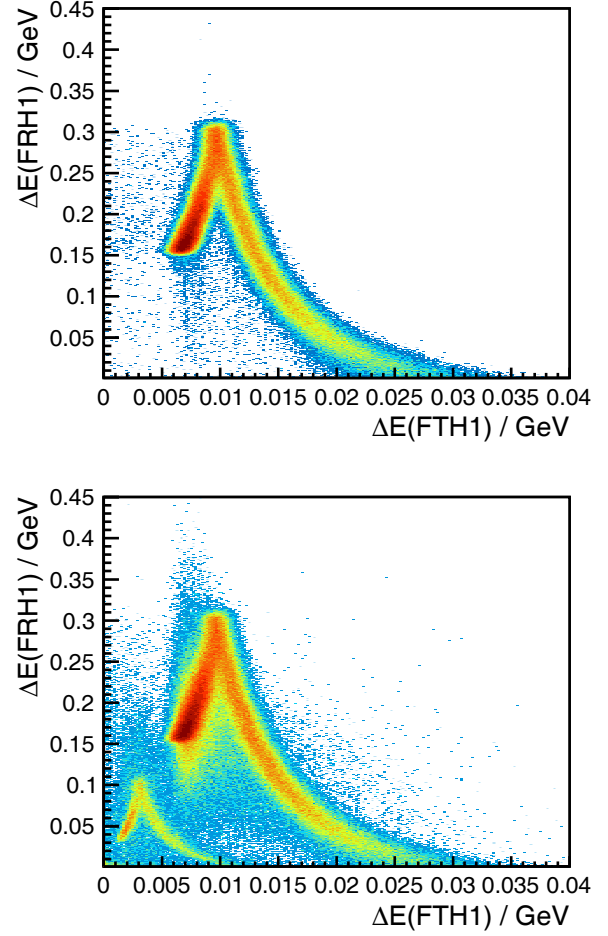


Fig. 6. Energy loss in the first layer of the Forward Range Hodoscope as a function of the energy loss in the preceding Forward Trigger Hodoscope from a Monte Carlo simulation of ${}^3\text{He}$ nuclei in the WASA Forward Detector with equally distributed values of kinetic energy and polar scattering angle between $0.1\text{ GeV} \leq T_{{}^3\text{He}} \leq 0.9\text{ GeV}$ and $2^\circ \leq \vartheta \leq 20^\circ$, respectively. Top: unmodified GEANT3 simulation. Bottom: including the modifications developed by the authors of [17]. The colour axis, representing intensity, is arbitrarily scaled and logarithmic.

reveals both an additional energy loss band resulting from singly charged protons produced in discrete breakup processes and an additional energy loss smearing to smaller ΔE .

The acceptance for a given reaction is influenced by both of these effects. A discrete breakup will lead to an identification of a proton instead of a ${}^3\text{He}$ nucleus, whereas the additional source of energy-loss smearing leads to wrongly reconstructed kinetic energies and thus to event reconstruction away from the expected final state momentum (or missing-mass) peak position. As the probability for such processes to occur scales with the path length through the detector material and, thus, with initial ${}^3\text{He}$ kinetic energy, backward single pion production is more heavily affected than, *e.g.*, η meson production.

Appendix B. Cross section values

Table 2. Values in nb/sr of the $pd \rightarrow {}^3\text{He}\pi^0$ differential cross sections shown graphically in fig. 5 from beam momenta of 1600 MeV/c to 1670 MeV/c. The bins in $z = \cos\vartheta_{\pi^0}^*$ have width 0.016 and the values quoted are the centres of these bins. Statistical uncertainties are given.

z	1600	1610	1620	1630	1640	1650	1660	1670
-0.976	20.4 ± 1.0	19.5 ± 1.0	17.6 ± 0.9	18.3 ± 0.9	20.3 ± 1.0	20.4 ± 1.0	20.0 ± 1.1	20.1 ± 1.0
-0.960	28.1 ± 1.2	24.7 ± 1.0	22.6 ± 1.0	20.5 ± 0.9	20.5 ± 1.0	20.3 ± 0.9	21.7 ± 1.0	21.2 ± 0.9
-0.944	34.1 ± 1.2	31.3 ± 1.1	24.1 ± 1.0	25.2 ± 1.0	24.8 ± 1.0	22.7 ± 0.9	22.7 ± 1.0	23.2 ± 1.0
-0.928	39.9 ± 1.3	33.3 ± 1.1	29.1 ± 1.1	27.9 ± 1.0	29.8 ± 1.1	27.8 ± 1.0	26.7 ± 1.1	26.6 ± 1.0
-0.912	44.2 ± 1.3	40.3 ± 1.1	34.7 ± 1.1	32.1 ± 1.0	34.9 ± 1.1	29.7 ± 1.0	30.2 ± 1.1	28.3 ± 1.0
-0.896	53.4 ± 1.4	45.9 ± 1.2	40.5 ± 1.2	37.0 ± 1.1	38.1 ± 1.2	35.7 ± 1.1	32.6 ± 1.2	32.5 ± 1.1
-0.880	58.8 ± 1.5	51.2 ± 1.3	42.1 ± 1.2	40.6 ± 1.1	41.3 ± 1.2	39.1 ± 1.1	38.3 ± 1.2	34.2 ± 1.1
-0.864	63.0 ± 1.5	55.5 ± 1.3	47.4 ± 1.3	45.1 ± 1.2	46.2 ± 1.3	43.9 ± 1.2	41.0 ± 1.3	40.4 ± 1.2
-0.848	66.6 ± 1.5	58.1 ± 1.3	50.3 ± 1.3	49.7 ± 1.2	48.9 ± 1.3	49.1 ± 1.3	46.9 ± 1.3	42.6 ± 1.2
-0.832	69.2 ± 1.6	61.6 ± 1.4	55.4 ± 1.3	54.9 ± 1.3	54.1 ± 1.4	50.6 ± 1.3	49.8 ± 1.4	45.3 ± 1.3
-0.816	75.1 ± 1.6	64.9 ± 1.4	59.1 ± 1.4	56.0 ± 1.3	58.3 ± 1.4	55.4 ± 1.3	52.6 ± 1.4	47.9 ± 1.3
-0.800	77.9 ± 1.7	69.8 ± 1.5	61.3 ± 1.4	59.1 ± 1.3	59.7 ± 1.4	57.4 ± 1.4	55.3 ± 1.4	52.6 ± 1.3
-0.784	81.4 ± 1.7	70.4 ± 1.5	64.0 ± 1.5	62.0 ± 1.4	61.9 ± 1.4	60.3 ± 1.4	60.0 ± 1.5	56.8 ± 1.3
-0.768	83.0 ± 1.7	75.9 ± 1.5	64.7 ± 1.4	64.7 ± 1.4	68.1 ± 1.5	64.0 ± 1.4	65.0 ± 1.5	58.6 ± 1.4
-0.752	85.4 ± 1.7	78.2 ± 1.5	68.5 ± 1.5	66.8 ± 1.4	68.3 ± 1.5	66.5 ± 1.5	66.6 ± 1.5	61.4 ± 1.4
-0.736	91.7 ± 1.8	78.6 ± 1.5	72.8 ± 1.5	70.0 ± 1.4	74.1 ± 1.5	70.7 ± 1.5	68.4 ± 1.6	65.4 ± 1.4
-0.720	90.5 ± 1.8	80.3 ± 1.5	73.1 ± 1.5	71.1 ± 1.4	73.2 ± 1.5	70.5 ± 1.5	74.4 ± 1.6	68.5 ± 1.4
-0.704	93.6 ± 1.8	83.6 ± 1.6	76.2 ± 1.5	73.4 ± 1.4	77.6 ± 1.6	72.7 ± 1.5	76.4 ± 1.6	70.7 ± 1.5
-0.688	96.2 ± 1.8	85.6 ± 1.6	75.6 ± 1.5	74.8 ± 1.4	77.9 ± 1.6	78.3 ± 1.5	74.0 ± 1.6	72.0 ± 1.5
-0.672	93.9 ± 1.8	86.5 ± 1.6	76.4 ± 1.5	77.0 ± 1.5	79.6 ± 1.6	78.2 ± 1.5	78.2 ± 1.6	74.4 ± 1.5
-0.656	92.4 ± 1.8	88.3 ± 1.6	78.5 ± 1.5	77.2 ± 1.5	79.0 ± 1.6	79.4 ± 1.5	77.4 ± 1.6	77.0 ± 1.5
-0.640	–	87.5 ± 1.6	78.1 ± 1.5	76.8 ± 1.5	79.7 ± 1.6	80.1 ± 1.5	77.6 ± 1.6	75.2 ± 1.5
-0.624	–	–	75.3 ± 1.5	76.6 ± 1.4	82.5 ± 1.6	79.4 ± 1.5	78.2 ± 1.6	77.9 ± 1.5
-0.608	–	–	77.0 ± 1.5	78.5 ± 1.5	83.3 ± 1.6	82.7 ± 1.6	80.3 ± 1.6	76.3 ± 1.5
-0.592	–	–	–	72.4 ± 1.4	82.7 ± 1.6	81.8 ± 1.5	77.4 ± 1.6	76.0 ± 1.5
-0.576	–	–	–	–	79.5 ± 1.6	78.9 ± 1.5	78.2 ± 1.6	77.8 ± 1.5
-0.560	–	–	–	–	–	76.4 ± 1.5	77.6 ± 1.5	74.2 ± 1.4
-0.544	–	–	–	–	–	–	73.2 ± 1.5	74.7 ± 1.4
-0.528	–	–	–	–	–	–	–	70.2 ± 1.4
-0.512	–	–	–	–	–	–	–	67.6 ± 1.4

Table 3. Values in nb/sr of the $pd \rightarrow {}^3\text{He}\pi^0$ differential cross sections shown graphically in fig. 5 from beam momenta of 1680 MeV/c to 1740 MeV/c. The bins in $z = \cos\vartheta_{\pi^0}^*$ have width 0.016 and the values quoted are the centres of these bins. Statistical uncertainties are given.

z	1680	1690	1700	1710	1720	1730	1740
-0.976	19.0 ± 1.0	21.0 ± 1.0	21.6 ± 0.6	22.8 ± 1.0	21.4 ± 1.2	24.1 ± 1.1	22.6 ± 1.1
-0.960	19.9 ± 1.0	20.2 ± 0.9	19.8 ± 0.5	19.9 ± 1.0	19.7 ± 1.1	20.3 ± 0.9	20.2 ± 1.0
-0.944	20.2 ± 1.0	21.7 ± 0.9	19.5 ± 0.5	20.0 ± 1.0	21.3 ± 1.0	19.9 ± 0.9	17.2 ± 0.9
-0.928	23.4 ± 1.0	23.2 ± 0.9	20.1 ± 0.5	20.0 ± 0.9	21.1 ± 1.0	19.3 ± 0.9	18.8 ± 0.9
-0.912	24.8 ± 1.0	23.5 ± 0.9	21.9 ± 0.5	21.0 ± 0.9	22.3 ± 1.0	19.9 ± 0.9	19.0 ± 1.0
-0.896	28.9 ± 1.1	27.7 ± 1.0	23.6 ± 0.6	23.9 ± 1.0	23.7 ± 1.0	21.5 ± 0.9	21.5 ± 1.0
-0.880	31.2 ± 1.1	28.2 ± 1.0	25.5 ± 0.6	24.8 ± 1.0	25.3 ± 1.1	21.7 ± 0.9	22.1 ± 1.0
-0.864	38.1 ± 1.2	31.9 ± 1.1	28.5 ± 0.6	30.1 ± 1.1	29.0 ± 1.1	24.0 ± 1.0	25.6 ± 1.0
-0.848	38.4 ± 1.2	33.6 ± 1.1	32.4 ± 0.6	31.1 ± 1.1	30.3 ± 1.1	27.3 ± 1.0	27.4 ± 1.1
-0.832	42.4 ± 1.3	39.9 ± 1.2	36.1 ± 0.7	36.3 ± 1.2	34.5 ± 1.2	29.3 ± 1.1	29.1 ± 1.1
-0.816	46.9 ± 1.3	44.1 ± 1.2	37.9 ± 0.7	39.2 ± 1.2	38.2 ± 1.3	32.2 ± 1.1	31.3 ± 1.1
-0.800	48.2 ± 1.3	47.9 ± 1.2	40.8 ± 0.7	43.8 ± 1.3	40.9 ± 1.3	34.6 ± 1.1	36.4 ± 1.2
-0.784	53.4 ± 1.4	50.3 ± 1.3	43.2 ± 0.7	46.1 ± 1.3	44.9 ± 1.3	39.0 ± 1.2	37.6 ± 1.2
-0.768	57.7 ± 1.4	54.3 ± 1.3	46.6 ± 0.7	46.8 ± 1.3	47.5 ± 1.4	42.9 ± 1.2	40.5 ± 1.2
-0.752	62.3 ± 1.5	55.3 ± 1.3	50.2 ± 0.8	50.0 ± 1.3	51.0 ± 1.4	45.7 ± 1.2	46.3 ± 1.3
-0.736	63.4 ± 1.5	59.4 ± 1.4	53.8 ± 0.8	54.0 ± 1.4	55.7 ± 1.5	48.5 ± 1.3	48.6 ± 1.3
-0.720	68.8 ± 1.5	62.3 ± 1.4	56.5 ± 0.8	57.9 ± 1.4	55.9 ± 1.4	51.3 ± 1.3	51.6 ± 1.4
-0.704	69.8 ± 1.5	66.6 ± 1.4	58.8 ± 0.8	62.4 ± 1.4	59.6 ± 1.5	53.6 ± 1.3	53.4 ± 1.4
-0.688	69.5 ± 1.5	68.8 ± 1.4	60.0 ± 0.8	61.1 ± 1.4	60.8 ± 1.5	55.4 ± 1.3	57.8 ± 1.4
-0.672	71.1 ± 1.5	68.2 ± 1.4	60.8 ± 0.8	65.8 ± 1.5	63.6 ± 1.5	57.0 ± 1.3	59.8 ± 1.4
-0.656	75.2 ± 1.6	68.7 ± 1.4	62.0 ± 0.8	65.2 ± 1.5	62.9 ± 1.5	58.4 ± 1.3	58.6 ± 1.4
-0.640	75.7 ± 1.6	69.8 ± 1.4	60.9 ± 0.8	68.7 ± 1.5	65.6 ± 1.5	58.9 ± 1.3	59.7 ± 1.4
-0.624	76.5 ± 1.6	68.9 ± 1.4	63.2 ± 0.8	66.2 ± 1.4	65.2 ± 1.5	60.4 ± 1.4	60.5 ± 1.4
-0.608	77.7 ± 1.6	68.8 ± 1.4	62.5 ± 0.8	64.9 ± 1.4	65.4 ± 1.5	59.9 ± 1.3	60.5 ± 1.4
-0.592	74.9 ± 1.5	67.7 ± 1.4	62.2 ± 0.8	66.7 ± 1.4	63.4 ± 1.5	59.5 ± 1.3	60.5 ± 1.4
-0.576	79.1 ± 1.6	68.1 ± 1.4	61.5 ± 0.8	68.3 ± 1.4	63.9 ± 1.5	60.7 ± 1.3	58.6 ± 1.4
-0.560	75.6 ± 1.6	65.9 ± 1.3	59.1 ± 0.8	63.6 ± 1.4	63.5 ± 1.4	57.8 ± 1.3	56.8 ± 1.4
-0.544	77.2 ± 1.6	64.6 ± 1.3	59.4 ± 0.8	63.4 ± 1.4	61.3 ± 1.4	58.4 ± 1.3	56.0 ± 1.3
-0.528	73.7 ± 1.5	63.5 ± 1.3	56.4 ± 0.7	60.0 ± 1.3	58.0 ± 1.3	58.8 ± 1.3	52.0 ± 1.3
-0.512	70.1 ± 1.5	60.4 ± 1.2	54.9 ± 0.7	60.4 ± 1.3	55.8 ± 1.3	56.3 ± 1.3	50.9 ± 1.2
-0.496	66.4 ± 1.4	61.5 ± 1.2	51.1 ± 0.7	55.6 ± 1.3	55.6 ± 1.3	51.7 ± 1.2	48.5 ± 1.2
-0.480	–	53.0 ± 1.2	49.7 ± 0.7	52.4 ± 1.2	50.7 ± 1.2	47.7 ± 1.1	43.1 ± 1.1
-0.464	–	–	44.2 ± 0.6	46.2 ± 1.1	47.3 ± 1.2	43.9 ± 1.1	40.2 ± 1.1
-0.448	–	–	–	40.8 ± 1.0	41.4 ± 1.1	40.3 ± 1.1	37.2 ± 1.0
-0.432	–	–	–	–	35.8 ± 1.0	36.0 ± 1.0	30.6 ± 0.9
-0.416	–	–	–	–	–	27.4 ± 0.9	25.9 ± 0.8

References

1. P. Berthet *et al.*, Nucl. Phys. A **443**, 589 (1985).
2. C. Kerboul *et al.*, Phys. Lett. B **181**, 28 (1986).
3. J.W. Low *et al.*, Phys. Rev. C **23**, 1656 (1981).
4. E. Aslanides *et al.*, Phys. Rev. Lett. **39**, 1654 (1977).
5. J. Banaigs *et al.*, Phys. Lett. B **45**, 394 (1973).
6. P. Adlarson *et al.*, Eur. Phys. J. A **50**, 100 (2014).
7. P. Adlarson *et al.*, Phys. Rev. C **91**, 015201 (2015).
8. P. Adlarson *et al.*, Phys. Lett. B **782**, 297 (2018).
9. M. Ruderman, Phys. Rev. **87**, 383 (1952).
10. W.R. Falk, Phys. Rev. C **61**, 034005 (2000).
11. L. Canton, L.G. Levchuk, Phys. Rev. C **71**, 014001 (2005).
12. J.-F. Germond, C. Wilkin, J. Phys. G **16**, 381 (1990).
13. J.M. Laget, J.-F. Lecomte, Phys. Lett. B **194**, 177 (1987).
14. H.-H. Adam *et al.*, *Proposal for the wide angle shower apparatus (WASA) at COSY-Jülich: WASA at COSY*, (2004), arXiv:nucl-ex/0411038.
15. R. Maier, Nucl. Instrum. Methods A **390**, 18 (1997).
16. R. Brun *et al.*, *GEANT Detector Description and Simulation Tool* (1994) <https://cds.cern.ch/record/1082634/files/geantall.CERN-W5013.pdf>.
17. R. Bilger *et al.*, Phys. Rev. C **65**, 044608 (2002).
18. T. Rausmann *et al.*, Phys. Rev. C **80**, 017001 (2009).
19. N. Hüskens, *η and π^0 production in proton-deuteron fusion to $^3\text{He} X$ with WASA-at-COSY*, PhD Thesis, Westfälische Wilhelms-Universität Münster, Germany (2017).
20. B. Mayer *et al.*, Phys. Lett. B **181**, 25 (1986).
21. J. Smyrski *et al.*, Phys. Lett. B **649**, 258 (2007).
22. T. Mersmann *et al.*, Phys. Rev. Lett. **98**, 242301 (2007).
23. C. Wilkin, Phys. Rev. C **47**, R938 (1993).
24. J.C. Peng *et al.*, Phys. Rev. Lett. **63**, 2353 (1989).